

ORIGINAL ARTICLE

DUOX2 promotes the progression of colorectal cancer cells by regulating the AKT pathway and interacting with RPL3

Xue Zhang^{1,2}, Jing Han^{1,2}, Li Feng¹, Lianghui Zhi², Da Jiang¹, Bin Yu², Zhenya Zhang², Bo Gao², Cong Zhang³, Meng Li², Lianmei Zhao^{3,*} and Guiying Wang^{2,4,*}

¹Department of Medical Oncology, Hebei Medical University Fourth Affiliated Hospital, Shijiazhuang 050000, Hebei, China,

²The Second General Surgery, Hebei Medical University Fourth Affiliated Hospital, Shijiazhuang 050000, Hebei, China,

³Scientific Research Center, Hebei Medical University Fourth Affiliated Hospital, Shijiazhuang 050000, Hebei, China and

⁴Department of General Surgery, Hebei Medical University Third Affiliated Hospital, Shijiazhuang 050000, Hebei, China

*To whom correspondence should be addressed. Tel: +86 0311 86095347; Fax: +86 0311 86032788; Email: wangguiyingtgy@163.com

Correspondence may also be addressed to Lianmei Zhao. Tel: +86 0311 86095290; Fax: +86 0311 86032788; Email: zhaolianmei@hbydsy.com

Abstract

Dual oxidase 2 (DUOX2) is an important regulatory protein in the organic process of thyroid hormone iodine. Mounting evidence suggests that DUOX2 plays a crucial role in the occurrence and development of cancers. However, the function and mechanism of DUOX2 in colorectal cancer (CRC) have not been fully clarified. In the present study, the relationship between the expression of DUOX2 and the clinicopathological features and prognosis of CRC patients was analyzed. Furthermore, the effects of DUOX2 on proliferation and invasion *in vitro* and *in vivo* were examined. DUOX2-associated proteins were identified by immunoprecipitation (IP). Next-generation sequencing detection was performed to illustrate the mechanism of DUOX2 in CRC cells. It was found that the expression levels of DUOX2 in metastatic sites were significantly higher than those in primary tumor tissues, and this was demonstrated to be associated with poor prognosis. The knockdown of DUOX2 inhibited the invasion and migration of CRC cells. Furthermore, DUOX2 regulated the stability of ribosomal protein uL3 (RPL3) by affecting the ubiquitination status of RPL3, and the invasion and migration ability of DUOX2 can be reversed by the overexpression of RPL3. The downregulation of DUOX2 can affect the expression level of a large number of genes, and a number of these are enriched in the PI3K–AKT pathway. Some of the changes caused by DUOX2 can be reversed by RPL3. In summary, DUOX2 exhibits a significantly higher expression in CRC tumor samples, and facilitates the invasion and metastasis ability of CRC cells by interacting with RPL3.

Introduction

Colorectal cancer (CRC) is one of the most common malignancies worldwide, and the second leading cause of tumor death (1). With the aging of the population and the change in lifestyle, the incidence of CRC is gradually increasing worldwide, which seriously endangers human health. Among the malignant tumors in China, the incidence and mortality rate of CRC ranks the top five, and approximately 60% of these patients are diagnosed in the middle and late stage (2). The 5-year survival rate of early stage patients can reach approximately 90%, while that

of advanced patients is merely less than 10% (3). Once recurrence and metastasis occur, the survival of CRC patients would be greatly threatened. Therefore, there is an urgent need to identify novel metastasis-related biomarkers for CRC.

DUOX2 belongs to the NADPH oxidase (NOX) family. In this family, there are other six members: DUOX1, NOX1, NOX2, NOX3, NOX4 and NOX5. DUOX1 and DUOX2 genes are located on human chromosome 15, which are two closely related isoforms, and were originally discovered in the thyroid gland (4). These are

Received: April 21, 2020; Revised: May 28, 2020; Accepted: June 8, 2020

© The Author(s) 2020. Published by Oxford University Press.

This is an Open Access article distributed under the terms of the Creative Commons Attribution Non-Commercial License (<http://creativecommons.org/licenses/by-nc/4.0/>), which permits non-commercial re-use, distribution, and reproduction in any medium, provided the original work is properly cited. For commercial re-use, please contact journals.permissions@oup.com

Abbreviations

CRC	colorectal cancer
IP	immunoprecipitation
MS	mass spectrometry
ROS	reactive oxygen species
WB	western blot

associated with thyroid dysmorphogenesis and genetic transient congenital hypothyroidism (5–7). The NOX family plays a different role in the carcinogenesis process. Recent studies have revealed that *DUOX2* is upregulated in liver cancer (8), pancreatic cancer (9–11) and prostate cancer (12), while this is downregulated in lung cancer (13). In addition, *DUOX2* may affect the therapeutic effect of gastrointestinal cancer (14,15). However, the role of *DUOX2* in CRC remains unclear. The present study aims to clarify the role of *DUOX2* in the invasion and metastasis of CRC, and its possible mechanism.

In the previous study conducted by the investigators, 11 pairs of cancer tissues and normal tissues were compared, and it was demonstrated that 1606 mRNAs are highly expressed in cancer tissues, when compared with para-cancer tissues (GSE104836) (16). In a further study, three CRC patients with lymphatic metastasis and six CRC patients without lymphatic metastasis were compared. It was found that *DUOX2* is more highly expressed in CRC tissues, when compared with para-cancer tissues, and is also more highly expressed in cancer tissues with lymph node metastasis, when compared with cancer tissues without lymph node metastasis. In the present study, the effect of *DUOX2* on the phenotype of CRC cells *in vitro* and *in vivo* was evaluated. Finally, the potential mechanism of dual oxidase 2 (*DUOX2*) in interacting with ribosomal protein uL3 (*RPL3*) to promote the development of CRC was revealed.

Materials and methods

Human CRC tissue samples

Fresh tissue specimens were collected from 89 CRC patients from Hebei Medical University Fourth Affiliated Hospital (Hebei, China), between 2018 and 2019, for the real-time quantitative reverse-transcription polymerase chain reaction (qRT-PCR) test. All 89 paired CRC tissue samples included para-cancer tissue specimens (at least 5 cm away from the edge of the tumor mass) and cancer tissue specimens (confirmed by pathological diagnosis). In addition, the paraffin specimens of 50 metastatic CRC (mCRC) patients between 2010 and 2014 were collected for the immunohistochemical (IHC) test. All mCRC patients had lymph nodes and liver metastases, and underwent resection of the primary lesion and metastatic liver. Then, the clinicopathological features were simultaneously summarized. The present study was approved by the Ethics Review Board of Hebei Provincial Tumor Hospital, and a signed informed consent was provided by all subjects.

The qRT-PCR

Total RNA was extracted using TRIzol Reagent (Thermo, Waltham, MA), and reverse-transcribed into complementary DNA (cDNA) with the same RNA concentration for each sample using the Reverse Transcription System (Promega, Fitchburg, WI), according to the manufacturer's instructions. Then, the prepared cDNA was subjected to quantitative PCR (qPCR) analysis using the 7500 RT-PCR System (AB Applied Biosystems) with the qPCR Mix (Promega, Madison, WI). Real-time PCR assays were performed to quantify the mRNA levels of *DUOX2*, *DUOX2A*, *CCDC113*, *PODXL2*, *PDZK1IP1*, *SYNE4*, *SHH*, *MAGEA3*, *RPL3*, *MYC*, *AKT1*, *EGFR* and *GAPDH*. The comparative Ct method ($\Delta\Delta Ct$) was used to analyze relative expression of genes. The fold change was evaluated as $2^{-\Delta\Delta Ct}$. Three technical replicates per sample were presented. The primers for *CCDC113*, *PODXL2*, *PDZK1IP1*, *SYNE4*, *SHH* and *MAGEA3* were purchased from GeneCopia (Rockville, MD), and the product IDs were HQP063033, HQP012148, HQP000201, HQP071160,

HQP017098 and HQP010978, respectively. The other primer sequences are presented in [Supplementary Table 1](#), available at [Carcinogenesis Online](#).

IHC staining

IHC staining was performed to analyze the expression of *DUOX2* in the 50 collected mCRC samples. In order to further explore the relationship between *DUOX2* and *RPL3*, tissue microarrays were used, which consisted of 35 pairs of CRC tissues and adjacent tissues. Antibodies against *DUOX2* (Bioss, Beijing, China) or *RPL3* (Proteintech, Wuhan, China) were applied at a dilution of 1:200. The IHC results were independently assessed by at least two pathologists. Each section was scored according to the intensity of the staining and the percentage of positive cells, respectively. The staining intensity was scored, as follows: 0 (negative), 1 (weak staining), 2 (moderate intense staining) or 3 (strong staining). The extent of the staining was scored based on the percentage of positive cells: 0 ($\leq 5\%$), 1 (6–25%), 2 (26–50%), 3 (50–75%) and 4 ($> 75\%$). The final IHC score was obtained by multiplying the intensity and percentage scores.

Hematoxylin and eosin (H&E) staining

The paraffin sections were dewaxed in water, and stained with hematoxylin dye solution (Servicebio, Wuhan, China) for 3–5 min. Then, these were washed by tap water, differentiated by differentiation solution (Servicebio, Wuhan, China), washed again by tap water, colored blue by the blue solution (Servicebio, Wuhan, China), and washed by water again. Afterwards, the sections were successively dehydrated with 85 and 95% gradient alcohol for 5 min, respectively, and stained with eosin dye (Servicebio, Wuhan, China) for 5 min. Finally, the tablet was dehydrated and sealed.

Western blot (WB) analysis

WB analysis was performed according to a previously described procedure (17). The antibody for *DUOX2* was purchased from ORIGENE Technologies (Rockville). The antibody for *RPL3* was purchased from BETHYL Laboratories (Montgomery). The antibodies for ubiquitin, *GAPDH*, E-cadherin and N-cadherin were purchased from Proteintech (Wuhan, China). The antibodies for *AKT*, c-MYC, *EGFR*, *MMP-2* and *MMP-9* were purchased from Cell Signaling Technology (Danfoss, Boston, MA). The antibody for p-AKT was purchased from Affinity (OH).

Cell culture

The SW480, SW620, HT29, HCT116 and DLD-1 CRC cell lines were purchased from the Type Culture Collection of the Chinese Academy of Science (Shanghai, China). NCM460, which is a normal human colon mucosa cell line, was obtained from INCELL (San Antonio, TX). All cell lines were authenticated using short tandem repeat profiling at the time of purchase. Next, SW480, SW620 and HT29 were cultured in Dulbecco's modified Eagle's medium (Thermo, MA, Waltham, MA). Then, NCM460, HCT116 and DLD-1 were cultured in RPMI-1640 medium (Thermo, Waltham, MA). Both kinds of medium contained 10% fetal bovine serum and 1% antibiotic. All experiments were performed with mycoplasma-free cells.

Transient transfection and stable transfection

DUOX2 was silenced in HCT116 and SW480 cells using siRNAs (Invitrogen, Carlsbad), according to the manufacturer's instructions. The target sequences were as follows: si1-*DUOX2*, 5'-GGAGGACAACAUGUGGUUTT AACCAUGAUGUUGUCCUCCTT-3'; si2-*DUOX2*, 5'-CCAUGAUGCGAUCUUC AUTTAUGAAGGAUCGCAUCAUGGTT-3'; si3-*DUOX2*, 5'-GCCAAAUGCUGUG UAAGAATTUUCUACACAGCAUUGGCTT-3'. The corresponding negative control RNA target sequence was 5'-UUCUCCGACGUGUCAGGUTTAGCU GACAGUUCGGAGAATT-3'. In order to stably knockdown *DUOX2* in cells, the siRNA targeting the si1-*DUOX2* coding sequence was designed and inserted into the lentiviral vector (Genechem Co., Ltd., Shanghai, China). A scramble siRNA was used as the negative control. The knockdown efficiencies were evaluated by qRT-PCR and WB analysis.

Plasmid transfection

In order to overexpress *DUOX2* and *RPL3* in cells, an expression construct was generated by subcloning the PCR-amplified full-length human *DUOX2* or *RPL3* cDNA into an EX-E1601-M02 or EX-F0331-M02 vector (GeneCopia,

Rockville, MD). An empty vector was used as the negative control. The overexpression efficiencies were evaluated by WB analysis.

Cell proliferation and viability assays

The colony-formation assay was carried out to evaluate the cell proliferation. Treated cells were seeded into a 6-well plate at 3000 cells/well, and cultured for 10 days. Then, the colonies were fixed with methanol and stained with crystal violet for 5–10 min, and the macroscopic colonies were counted. Cell viability was evaluated by 3-(4,5-dimethylthiazol-2-yl)-5-(3-carboxymethoxyphenyl)-2-(4-sulfophenyl)-2H-tetrazolium, inner salt (MTS) assay. Cells were cultured in 96-well plates at a density of 3000 cells/well, and this was performed using a MTS assay kit (Promega, Fitchburg, WI) for 3 days, according to the manufacturer's instructions.

Cell migration and Matrigel invasion assays

Cell migration and invasion assays were performed using the Transwell plate (Corning, NY) and wound scratch assay, respectively. For the invasion assays, the chamber inserts were coated with 60 μ l of Matrigel (BD, NJ), and dried for 12–16 h under sterile conditions in advance. Each upper chamber was plated with 1.5×10^5 cells, and each assay was repeated for three times. A microscope was used to quantify the number of migratory or invasive cells. The degree of invasion and migration was described as the number of treated cells. For the wound scratch assay, wound healing percentage was defined, as follows: (initial scratch area – certain time scratch area)/initial scratch area.

Immunoprecipitation (IP) and liquid chromatography–tandem mass spectrometry (LC–MS/MS)

The cell lysate of SW480 cells was obtained, and the total protein concentration was measured. Then, 1 mg of protein lysate supernatants and 30 μ l of precleared protein A/G beads (Roche, Switzerland) were mixed with 3 μ g of primary antibody (rabbit IgG and DUOX2, respectively), and incubated together at 4°C overnight. Then, the proteins were separated by sodium dodecyl sulfate–polyacrylamide gel electrophoresis. Afterwards, silver staining was performed. A significant band between 40 and 55 Kda was found on the gel, when compared with the control group. The LC–MS/MS analysis was carried out to identify the proteins from the samples. The Proteome discoverer software (version 1.4; Thermo Scientific) was used to the perform database search against the *Oryctolagus cuniculus* database (46 601 proteins) using the Sequest algorithm. The criteria were as follows: precursor mass tolerance of 15 ppm and fragment mass tolerance of 20 mmu. Then, the results were filtered using the following settings: merely high confident peptides with a global false discovery rate of <1% based on a target-decoy approach was included in the results. The procedures for the LC–MS/MS analysis were carried out by Capitalbio Technology Corporation (Beijing, China).

Coimmunoprecipitation

The total cell lysates of HCT116 and SW480 were, respectively, incubated with the appropriate antibodies and protein A/G beads at 4°C overnight. Then, the beads were washed six times using tissue/cell lysates, mixed with adequate amounts of protein loading buffer and boiled for 5–10 min. The coprecipitates were analyzed by WB analysis.

Animal experiments

The animal studies were conducted in accordance with the international standards-3R principle of animal welfare, and approved by the Experimental Animal Ethics Committee of Hebei Medical University Fourth Affiliated Hospital. Previously, two cell lines, which were stably knocked down of DUOX2 (i.e. HCT116 and HT29), were constructed. Five-week-old female BALB/c nude mice were randomly divided into different groups. For implantation, an equal number of HCT116 cells with DUOX2 knockdown or the corresponding negative control cells were resuspended in 150 μ l of PBS, and subcutaneously injected into the front flank ($n = 6$ /group) or caudal veins ($n = 5$ /group) of nude mice. In addition, an equal number of HT29 cells with DUOX2 knockdown, or the corresponding negative control cells were injected into the caudal veins ($n = 6$ /group). Finally,

the xenograft tumor, lung tissues and liver tissues were removed, photographed and weighed.

Statistical analysis

Almost each experiment was repeated for at least three times. The results were presented as mean \pm standard deviation. The differences between the groups were evaluated using two-tailed Student's *t*-test. The correlation analysis and survival data were analyzed using chi-square test, the Kaplan–Meier method (log-rank test) and Fisher's exact test. Kendall's tau-b analysis was used to analyze the correlation between DUOX2 and RPL3. The statistical analyses were performed using the GraphPad Prism 5.0 software (La Jolla, CA) and SPSS 21.0 software (SPSS). $P < 0.05$ was considered as statistically significant (* $P < 0.05$, ** $P < 0.01$ and *** $P < 0.001$).

Data availability

The datasets generated and analyzed in the present study are available in the GEO repository (GSE104836; <https://www.ncbi.nlm.nih.gov/geo/query/acc>) and (GSE139918; <https://www.ncbi.nlm.nih.gov/geo/query/acc>). The other data generated or analyzed in the present study are available from the corresponding author upon reasonable request.

Results

Gene screening and validation

A total of 3221 mRNAs were differentially expressed in CRC tissues, when compared with para-cancer tissues. These included 1606 upregulated mRNAs and 1615 downregulated mRNAs, according to the sequencing data shown in the previous study conducted by the investigators, which have been deposited in the GEO (GSE104836) (16). Compared with the cancer tissues of the six CRC patients without lymph node metastasis, 368 mRNAs were differentially expressed in the cancer tissues of three CRC patients with lymph node metastasis, which included 238 upregulated mRNAs and 130 downregulated mRNAs. Furthermore, nine overlap mRNAs were screened out, which were not only upregulated in CRC tissues, when compared with para-cancer tissues, but also upregulated in cancer tissues with lymph node metastasis, when compared with cancer tissues without lymph node metastasis. These mRNAs are listed as follows: *CCDC113*, *PODXL2*, *PDZK1IP1*, *SYNE4*, *SHH*, *MAGEA3*, *DUOX2*, *DUOXA2* and *NPFFR1* (Figure 1A). These were further verified by qRT-PCR in 24 pairs of CRC tissues and para-cancer tissues. *NPFFR1* was not successfully amplified, which may be due to the low expression of *NPFFR1* in CRC tissues. The results revealed that the expression of *CCDC113*, *PODXL2*, *SYNE4*, *DUOX2* and *DUOXA2* was significantly higher in CRC tissues than in para-cancer tissues, which is consistent with the results of the sequencing data. Among these, *DUOX2* was the most highly expressed, and this was selected for further study (Figure 1B). Then, the sample number was expanded to 89 pairs, and it was further confirmed that *DUOX2* mRNA was more highly expressed in CRC tissues, when compared with para-cancer tissues (Figure 1C). Among the 89 patients, 52 patients had no lymph node metastasis, while 37 patients had lymph node metastasis. Furthermore, the *DUOX2* mRNA expression was higher in CRC cancer tissues of patients with lymph node metastasis, when compared with that of patients without lymph node metastasis (Figure 1D). As summarized in Table 1, the relationship between the expression of *DUOX2* and the clinicopathological features of the 89 CRC patients was analyzed. These results revealed that the elevated expression of *DUOX2* was significantly associated with gender, tumor invasion, local lymph node metastasis and TNM stage, indicating that *DUOX2* may be correlated to CRC progression.

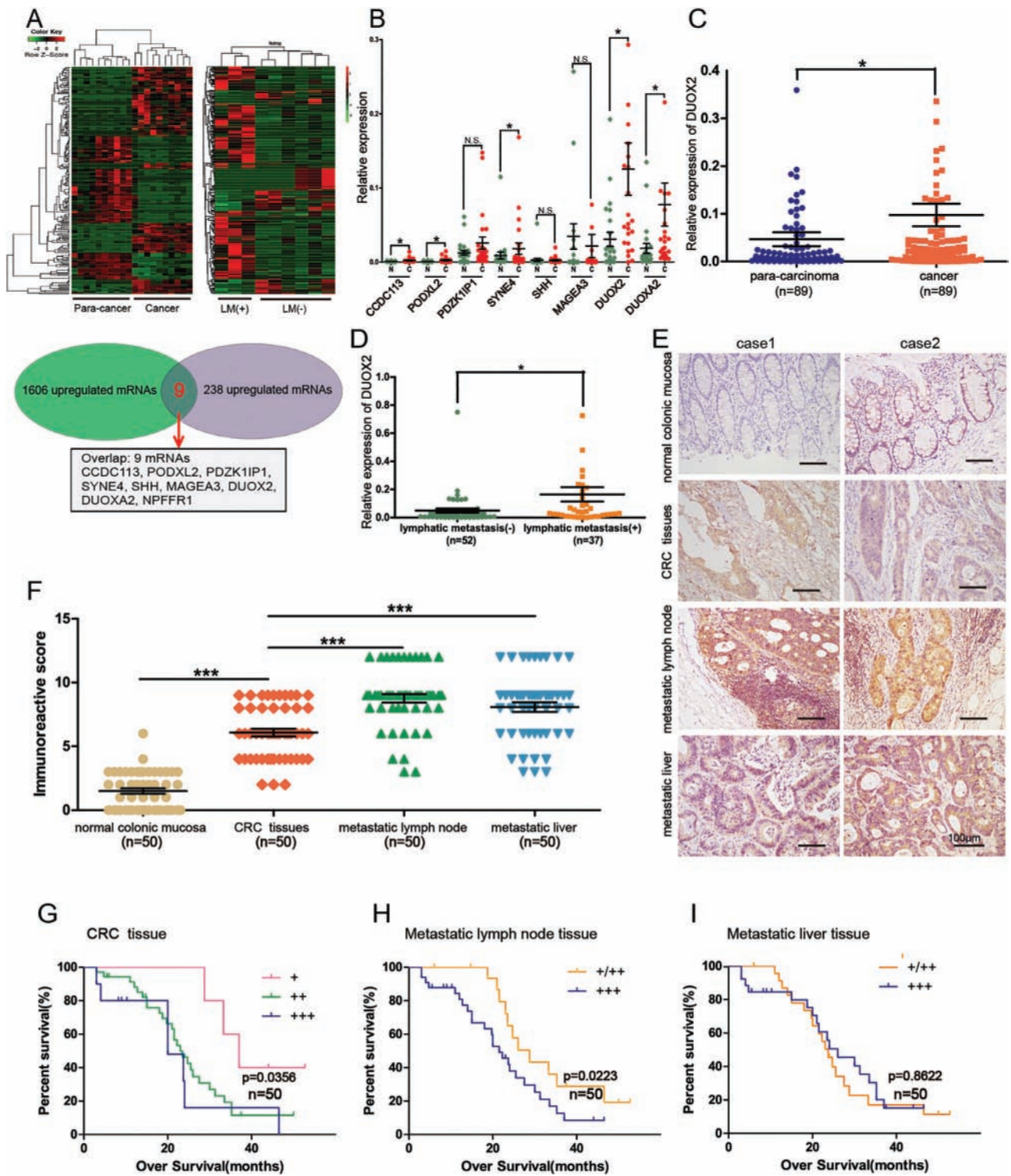


Figure 1. The expression of DUOX2 in CRC tissues and metastatic tumor tissues and its relationship with survival. (A) There were 1606 upregulated mRNAs in CRC tissues and 238 upregulated mRNAs in CRC tissues with lymph node metastasis. Make overlap and get nine mRNAs: CCDC113, PODXL2, PDZK1IP1, SYNE4, SHH, MAGEA3, DUOX2, DUOX2, and NPFFR1. (B) Candidate genes were validated by qRT-PCR. (C) DUOX2 expression was analyzed by qRT-PCR in 89 paired samples including para-carcinoma tissues and CRC tissues. Statistical analysis was performed using the paired-samples T-test. (D) It was also analyzed in CRC tissues without lymph node metastasis (n = 52) and CRC tissues with lymph node metastasis (n = 37). Independent-sample T-test was performed. (E) Representative immunohistochemistry staining of DUOX2 in normal colonic mucosa, CRC tissues, metastatic lymph node tissues and metastatic liver tissues (200x). (F) Comparison of the IHC scores of DUOX2 protein in different tissues (n = 50). (G) Overall survival analysis of DUOX2 expression in primary cancer tissues, (H) metastatic lymph node tissues and (I) metastatic liver tissues. *P < 0.05), ***P < 0.001.

Table 1. Correlation between DUOX2 expression and the clinicopathologic features in 89 CRC patients

Clinicopathologic features	n	DUOX2		χ^2	P-value
		Low	High		
All	89	44	45		
Age				0.623	0.43
≤60	34	15	19		
>60	55	29	26		
Gender				5.237	0.022*
Male	57	23	34		
Female	32	21	11		
Tumor site				0.023	0.879
Left	60	30	30		
Right	29	14	15		
Pathological type				0.734	0.392
Adenocarcinoma	76	39	37		
Non-adenocarcinoma	13	5	8		
Tumor size				0.012	0.913
<5 cm	43	21	22		
≥5 cm	46	23	23		
Tumor invasion				4.283	0.038*
T1 + T2	4	4	0		
T3 + T4	85	40	45		
N stage				5.183	0.023*
N0	52	31	21		
N1 + 2	37	13	24		
M stage				0.000	0.987
M0	87	43	44		
M1	2	1	1		
TNM stage				4.209	0.040*
I + II	51	30	21		
III + IV	38	14	24		
Tumor embolus				1.151	0.283
Negative	69	32	37		
Positive	20	12	8		
Nerve invasion				0.100	0.752
Negative	80	40	40		
Positive	9	4	5		
Pathological differentiation				0.764	0.382
Well moderate	83	40	43		
Poor	6	4	2		

The median expression level was used as the cutoff. Chi-square tests were used to analyze the correlation between the clinicopathologic features and the expression level of DUOX2.

*P < 0.05 indicates the statistical significance.

DUOX2 expression in mCRC tissues and metastatic tumor tissues and its relationship with survival

The DUOX2 protein expression was investigated in normal colonic mucosa, CRC tissues, metastatic lymph node tissues and metastatic liver tissues obtained from 50 cases (Figure 1E). The expression scores of DUOX2 in these collected tissues are presented in Supplementary Table 2, available at Carcinogenesis Online. This indicated that the order of the significant upregulation extent of the DUOX2 expression in metastatic lymph nodes and metastatic liver tissues was greater than primary cancer tissues ($P < 0.001$, Figure 1F) and greater than the normal colonic mucosa ($P < 0.000$). The Kaplan–Meier analysis revealed that higher DUOX2 expression in CRC tissues and metastatic lymph node tissues predicted the worse prognosis, when compared with lower DUOX2 expression, for mCRC patients (Figure 1G and H). However, the expression of DUOX2 in metastatic liver tissues was not correlated with overall survival (Figure 1I), which was probably due to the limited number of samples. Taken together, those results suggest that DUOX2 may

act as a metastasis promoting factor that contributes to the progression of CRC.

Effects of DUOX2 on invasion, metastasis and proliferation *in vitro*

In order to investigate the function of DUOX2, DUOX2 protein was detected in normal intestinal epithelium cell line NCM460 and five CRC cell lines, which included SW480, SW620, HCT116, HT-29 and DLD-1 (Figure 2A). Then, si1-DUOX2, si2-DUOX2, si3-DUOX2 and the negative control (si-NC) were transfected into HCT116 and SW480 cells. This revealed that si1-DUOX2 and si2-DUOX2 effectively downregulated the DUOX2 expression in HCT116 and SW480 cells (Figure 2B and C). Subsequently, the HCT116 and SW480 cell lines, which were transfected by si1-DUOX2 and si2-DUOX2, were used to perform MTS and colony formation, in order to investigate the effect of DUOX2 on proliferation. These results revealed that there was no significant difference in growth rate among the si1-DUOX2, si2-DUOX2 and si-NC groups, both in the HCT116 and SW480 cell lines

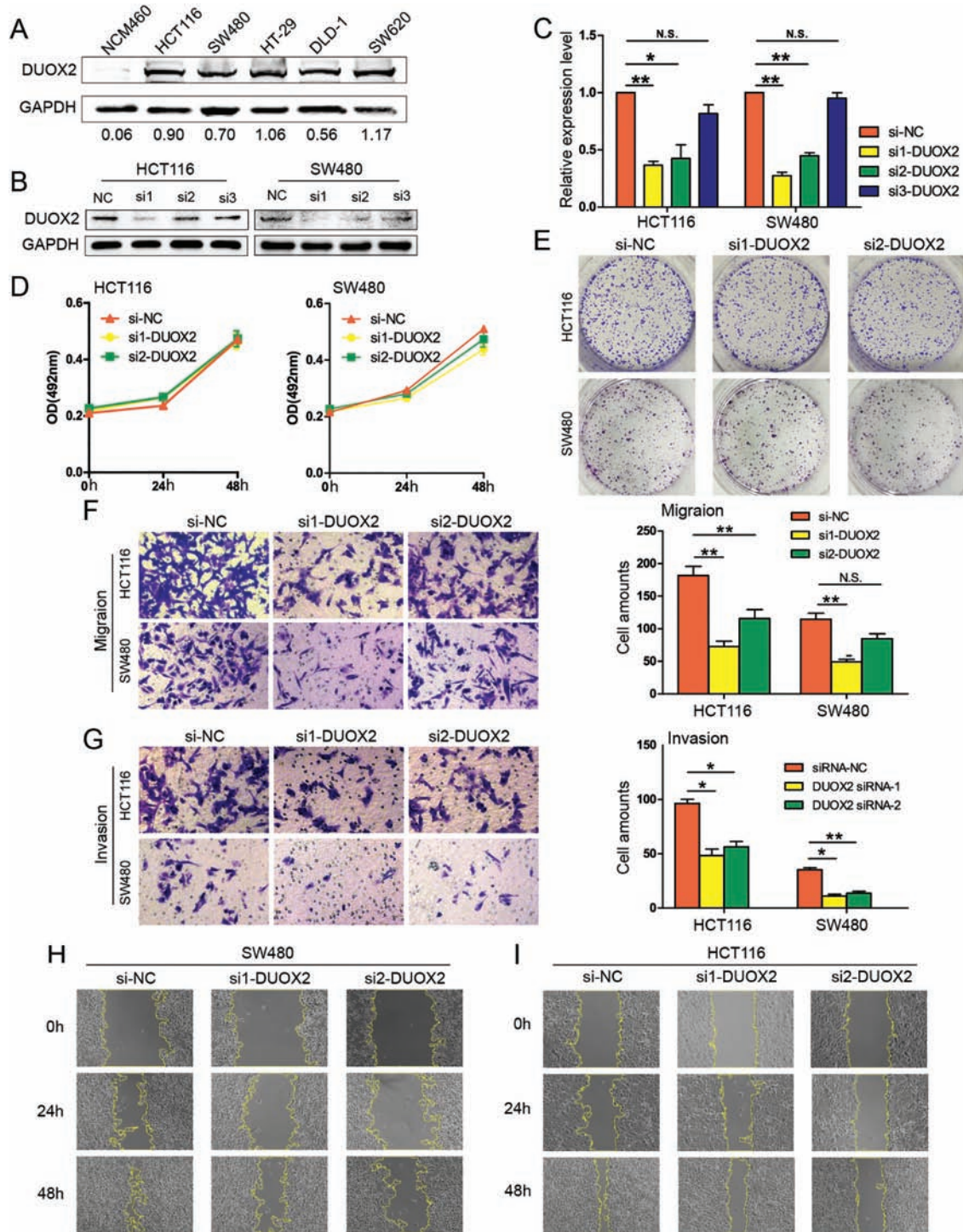


Figure 2. Knockdown of DUOX2 decreases the migration and invasion of CRC cells in vitro. (A) DUOX2 protein expression levels in one normal intestinal epithelium cell line and five CRC cell lines. (B and C) Western blotting and qRT-PCR were performed to detect the DUOX2 expression levels in DUOX2 knockdown (si1-DUOX2, si2-DUOX2 and si3-DUOX2) and negative control (si-NC). * $P < 0.05$, ** $P < 0.01$, $N.S.P > 0.05$. (D) MTS assay. DUOX2 knockdown did not attenuate the cell viability of HCT116 and SW480 cells. Each point indicates the mean of spectrometric absorbance $OD_{492} \pm SD$ of three independent experiments. (E) Colony assays. DUOX2 knockdown did not attenuate colony formation in HCT116 and SW480 cells. (F) Transwell migration assays. (G) Transwell invasion assays. The error bars represent the standard deviation. * $P < 0.05$, ** $P < 0.01$, $N.S.P > 0.05$. (H and I) Wound healing assay. The migration rate was derived from the ratio of the difference in wound area at different times to the initial wound area (200 \times). The tests were performed on SW480 and HCT116 cells. * $P < 0.05$, ** $P < 0.01$.

(Figure 2D). This was also consistent with the results of the colony-formation test (Figure 2E). In addition, the capacity of cell migration was determined by Transwell assay and wound healing assay. The invasion abilities of those cells were assessed

by Matrigel invasion assay. These results demonstrate that the amount of migrating cells and invading cells significantly decreased in both the si1-DUOX2 and si2-DUOX2 groups, when compared with the si-NC group, in both the HCT116 and SW480

cell lines (Figure 2F and G). The wound healing percentages also more significantly decreased in HCT116 and SW480 cells treated with si1-DUOX2 and si2-DUOX2, when compared with the si-NC group (Figure 2H and I, Supplementary Figure A, available at *Carcinogenesis* Online). Overall, those results indicate that the inhibition of DUOX2 can reduce the ability of CRC cells to invade and metastasize, but has no effect on proliferation.

The relationship between DUOX2 and RPL3

In order to further explore the underlying molecular mechanisms of DUOX2 in CRC cells, DUOX2-associated proteins were identified by IP. The differential band was observed to be specific to DUOX2, when compared with the IgG control, in the silver stained sodium dodecyl sulfate–polyacrylamide gel electrophoresis (Figure 3A). Next, the differential protein band was subjected to MS analysis (Report Number: JD-YX-2019-0184-JSFW-01). Among the candidate proteins shown in Supplementary Table 3, available at *Carcinogenesis* Online, RPL3 was chosen for further analysis due to its high score, and because its subcellular localization was consistent with the DUOX2 protein. Furthermore, it could stably interact with DUOX2, as validated by the WB analysis in HCT116 and SW480 cells (Figure 3B). In order to evaluate the relationship of DUOX2 with RPL3, the effect of DUOX2 on the expression level of RPL3 was initially investigated. The results revealed that the RPL3 protein expression was significantly upregulated after the downregulation of DUOX2, in both the HCT116 and SW480 cell lines (Figure 3C), while RPL3 did not significantly change in the gene level (Figure 3D). The qRT-PCR analysis of 23 CRC tissues revealed that there was no correlation between DUOX2 and RPL3 in the gene level (Figure 3E). However, the IHC results revealed that there was a negative correlation between DUOX2 and RPL3 protein in CRC tissues, metastatic lymph nodes and metastatic livers (Figure 3F and Supplementary Figure H, available at *Carcinogenesis* Online), suggesting that DUOX2 can regulate RPL3 at the protein level.

Accordingly, it was hypothesized that DUOX2 may regulate the RPL3 generation or degradation. Thus, cycloheximide, an inhibitor of protein synthesis to treat HCT116 and SW480 cells, was introduced, and this revealed that the RPL3 protein has a short half-life of approximately 4 h. Furthermore, when DUOX2 was knocked down, the rate of RPL3 protein degradation slowed down (Figure 3G). It was further hypothesized that the degradation of the RPL3 protein may be mediated by the ubiquitin–proteasome pathway. The sh-Control group and sh-DUOX2 group were treated with a proteasome inhibitor MG132, and the RPL3 protein levels were measured. Obviously, for cells not treated with MG132, the level of RPL3 protein significantly increased after DUOX2 was downregulated, but this trend disappeared after MG132 was added (Figure 3H). The protein levels of ubiquitin were detected by the WB test after the IP assay using the RPL3 antibody. As expected, polyubiquitin chains were detected in the RPL3 immune complex, and when DUOX2 protein levels were downregulated, the total number of polyubiquitin chains significantly decreased. The same volume of protein was extracted from each group for the WB analysis, with the anti-GAPDH antibody as the loading control (Figure 3I). These results suggest that DUOX2 may affect the RPL3 protein expression by affecting the ubiquitination status of RPL3.

RPL3 reverses the effects of DUOX2 *in vitro*

In order to further investigate the effects of DUOX2 and RPL3 on invasion and metastasis, a rescue test was designed, in which DUOX2 and RPL3 were successfully overexpressed after

transfecting plasmids into both HCT116 and SW480 cells (Figure 4A). Meanwhile, a negative control group was designed to avoid the interference. The Transwell results revealed that the migration and invasion abilities of HCT116 and SW480 cells significantly increased after overexpressing DUOX2, while the overexpression of RPL3 significantly reversed this trend (Figure 4B). These data indicated that RPL3 can reverse the effects of DUOX2 *in vitro*. Furthermore, the wound scratch assay was also carried out, and it was revealed that the migration ability was significantly enhanced after overexpressing DUOX2, while the trend disappeared after overexpressing DUOX2 and RPL3 at the same time (Figure 4C).

The knockdown of DUOX2 has a significant effect on the PI3K–AKT pathway

In order to illustrate the mechanism of DUOX2 in CRC cells, next-generation sequencing detection was performed on HCT116 cells transfected with si1-DUOX2, si2-DUOX2 and si-NC. The sequencing data were deposited in the GEO (GSE139918). It was found that there were many differentially expressed genes in the si1-DUOX2 group and si2-DUOX2 group, when compared with the si-NC group (Figure 4D). In order to clarify the biological functions of these genes *in vivo* and the involved signaling pathways, the enrichment analysis of the differential genes was conducted based on the KEGG database. In the present study, compared with the si-NC group, 48 differentially expressed genes in the si1-DUOX2 group and 25 differentially expressed genes in the si2-DUOX2 group were enriched in the phosphatidylinositol 3 kinase/protein kinase B (PI3K–AKT) signaling pathway (Figure 4E). Several metastasis-related genes in the PI3K–AKT pathway were selected for further validation. The results revealed that after the knockdown of DUOX2, the expression level of the EGFR gene significantly decreased, while the expression level of the AKT1 and MYC genes significantly increased (Figure 4F). Furthermore, it was also verified that after the overexpression of DUOX2, the EGFR protein levels increased, while the AKT, p-AKT and c-MYC protein levels significantly decreased. The increase in RPL3 protein level could not reverse the increase in EGFR, but could reverse the decrease in AKT, p-AKT and c-MYC. In addition, E-cadherin, which is known to be associated with invasion and metastasis, was selected for further investigation. These results revealed that with the increase in DUOX2 expression, the expression of E-cadherin significantly decreased. However, the overexpression of RPL3 can reverse the change in E-cadherin (Figure 4G).

Effects of DUOX2 on invasion and metastasis *in vivo*

In order to further study the role of DUOX2 *in vivo*, xenografts in nude mice were established using sh-DUOX2 and sh-Control stably infected HCT116 and HT-29 cells. More than 90% of these cells were successfully transfected with the lentivirus (Supplementary Figure B, available at *Carcinogenesis* Online). The results revealed that the expression of the DUOX2 gene and protein all significantly decreased after infection with sh-DUOX2 (Figure 5A and B). Furthermore, the lentivirus-infected HCT116 cells were transfected into the subcutaneous tissue of nude mice. Then, these nude mice were killed after 4 weeks, and the transplanted tumors were weighed. However, there was no significant difference in the weight of the transplanted tumors between the two groups (Supplementary Figure C and D, available at *Carcinogenesis* Online). In the sh-DUOX2 group, the expression of the DUOX2 protein significantly decreased, while the RPL3 expression significantly increased, further verifying that RPL3 is the target of DUOX2 (Figure 5C). After injecting the treated

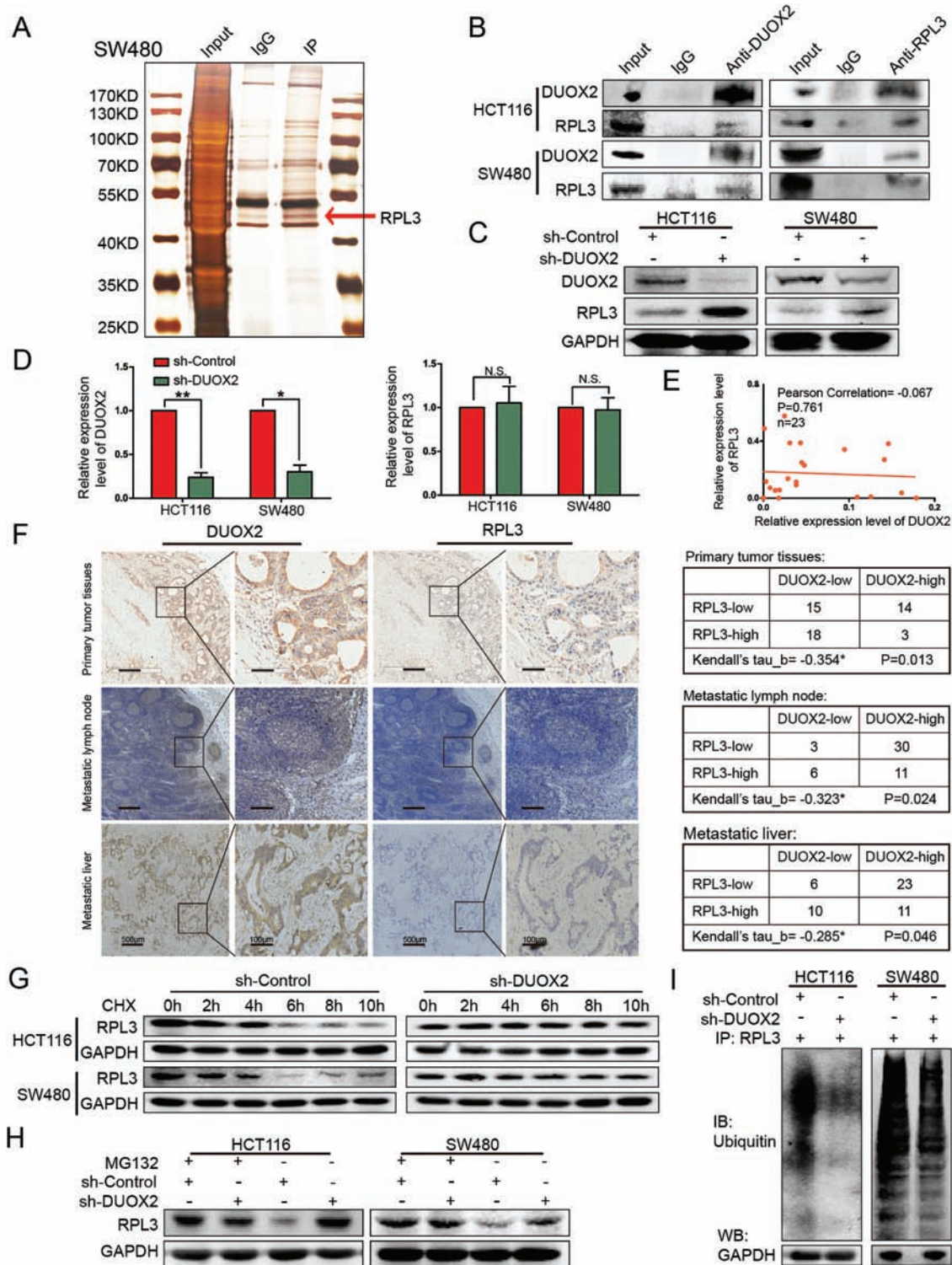


Figure 3. DUOX2 and RPL3 proteins are negatively correlated, DUOX2 interacts with RPL3 through ubiquitination. (A) The cell lysates were subjected to IP with anti-IgG antibody (IgG) or anti-DUOX2 antibody (IP). Differential bands between anti-DUOX2 and anti-IgG in the silver stained sodium dodecyl sulfate–polyacrylamide gel electrophoresis were detected by MS. (B) The interaction between DUOX2 and RPL3 was proved by means of coimmunoprecipitation. (C) Total protein of HCT116 and SW480 cells, which were knockdown DUOX2 (sh-DUOX2) and the negative control (sh-Control), was extracted and subjected to western blotting using anti-DUOX2, anti-RPL3 and anti-GAPDH antibodies. (D) The expression of RPL3 gene levels after DUOX2 knockdown in HCT116 and SW480 cells. (E) Expression of DUOX2 and RPL3 genes in CRC tissues ($n = 23$). Statistical analysis was performed using Pearson correlation coefficient. (F) The expressions of DUOX2 and RPL3 protein in different tissues of CRC patients by immunohistochemistry. Kendall's tau-b (Kendall) rank correlation coefficient was used to reflect the correlation between DUOX2 and RPL3 protein, $*P < 0.05$. (G) HCT116 and SW480 cells, which were knockdown DUOX2 (sh-DUOX2) and the negative control (sh-Control), were treated with cycloheximide (100 µg/ml), collected at the indicated time points and immunoblotted for RPL3 and GAPDH. (H) HCT116 and SW480 cells, which were knockdown DUOX2 (sh-DUOX2) and the negative control (sh-Control), were treated with MG132 (10 µM) for 12 h, total protein was extracted and subjected to western blotting using anti-RPL3 and anti-GAPDH antibodies. (I) Different groups of cells, sh-Control and sh-DUOX2, were lysed with IP lysis/wash buffer with protease inhibitor and phosphatase inhibitor. Anti-RPL3 antibody was used for IP, and the immune-precipitates were probed with anti-ubiquitin. The same volume of protein was extracted from each group for western blotting analysis with anti-GAPDH antibody as a loading control. $*P < 0.05$, $**P < 0.01$.

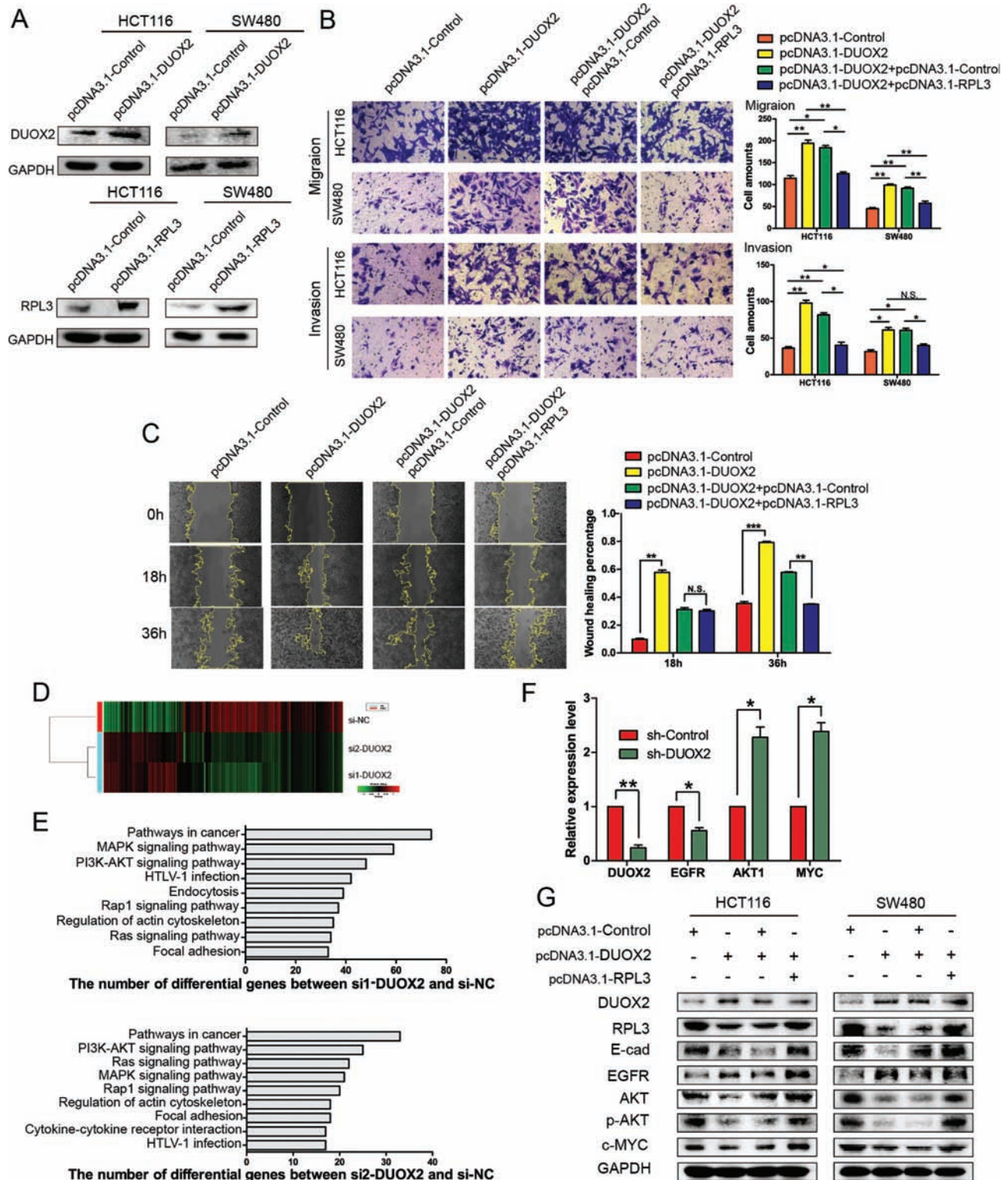


Figure 4. RPL3 reverses the effects of DUOX2 *in vitro*, and the different genes after DUOX2 knockdown were enriched in the AKT pathway, while RPL3 reversed this change partially. (A) Western blotting was performed to detect the DUOX2 protein in DUOX2-overexpressed (pcDNA3.1-DUOX2) and negative control (pcDNA3.1-Control) both in HCT116 and SW480 cells. (B) Transwell assays. The migration and invasion ability of the HCT116 and SW480 cells were significantly increased after overexpressing DUOX2, while the overexpression of RPL3 significantly reversed this trend. (C) Wound healing assay. The migration rate was derived from the ratio of the difference in wound area at different times to the initial wound area (200 \times). The tests were performed on SW480 cells. ^{N.S.P} > 0.05, **P* < 0.05, ***P* < 0.01, ****P* < 0.001. (D) Differentially expressed genes in DUOX2 knockdown (si1-DUOX2, si2-DUOX2) and negative control (si-NC) by next-generation sequencing as shown in the heatmap. (E) Different signaling pathways based on KEGG databases between si1-DUOX2 and si-NC group, or si2-DUOX2 and si-NC group. (F) Verification of related genes in PI3K-AKT pathway. (G) WB assay. The protein levels of E-cadherin (E-cad), EGFR, AKT, p-AKT, c-MYC after overexpression of DUOX2, or both of DUOX2 and RPL3.

HCT116 cells via the tail vein for 10 weeks, the nude mice were dissected ($n = 4/\text{group}$), while those injected with HT29 cells ($n = 6/\text{group}$) were dissected after 9 weeks. All lung and liver tissues were extracted (Supplementary Figure E and G, available at *Carcinogenesis* Online) and stained with H&E (Figure 5D). The statistical results demonstrated that the number of lung metastasis nodes and liver metastasis nodes significantly decreased after the knockdown of *DUOX2* (Figure 5E). Interestingly, the subcutaneous metastatic tumor node was also discovered in HT-29 cell-treated nude mice via the tail vein (Supplementary Figure F, available at *Carcinogenesis* Online). All metastatic tumors were removed and weighed. The H&E staining was performed to determine whether those metastatic tumors were metastatic lymph nodes. The results revealed that the nodules were infiltrated by cancer cells without lymph node structure (Figure 5G). Although there was no significant difference in the number of metastatic tumor nodes, the weight of the subcutaneous metastatic tumors was significantly lower in the sh-*DUOX2* group than in the sh-Control group ($P = 0.014$; Figure 5F and H).

Discussion

The present study focused on the biological functions of *DUOX2* in CRC, as well as the possible molecular mechanisms. The screening of the *DUOX2* gene was based on a previous next-generation sequencing result (16). In the present study, in order to better understand the role of *DUOX2* in CRC, the expression of *DUOX2* was analyzed at both the gene and protein level, and the expression was consistent with the results obtained during the screening process. The verification of these results at the gene level preliminarily confirmed that the expression of *DUOX2* in CRC tissues was significantly higher, when compared with that in para-cancer tissues, and that the increase in expression of *DUOX2* was significantly correlated to gender, tumor invasion, local lymph node metastasis and TNM stage. Due to the short follow-up time, the survival of the 89 CRC patients was not statistically analyzed. The IHC results for the mCRC patients revealed that the expression of *DUOX2* in the metastasis was significantly higher than that in primary cancer. Furthermore, the follow-up results revealed that the high protein expression of *DUOX2* indicates a short survival time. This conclusion is consistent with a previous literature (18). Therefore, it was considered that *DUOX2*, as an oncogene, is involved in the development of CRC.

A study revealed that (15) the expression of *DUOX2* is upregulated in 5-FU-resistant SNUC5 cells. Furthermore, the reactive oxygen species (ROS) produced by *DUOX2* can enhance the migration and invasion abilities of CRC cells. It has been well known that the microenvironment plays an important role in tumor development (19). The microenvironment of tumor cells is affected by a variety of factors. ROS, as the second messenger, is an important participant in cell signaling and regulation, which participates in the signal transduction process of gene transcription and protein synthesis, and plays an important role in the occurrence and development of tumors. An increase in ROS is one of the characteristics of cancer cells (20). ROS, such as H_2O_2 , is part of the gut's innate immune system in active enteritis, and plays an important role in maintaining mucosal barriers and protecting the host from pathogens (21,22). However, when intracellular ROS production exceeds the defense capacity of the intracellular antioxidant system, oxidative stress is caused. Long-term exposure of cells to oxidative stress can lead to abnormal signal transduction, which can promote the development of tumors (20). *DUOX2* has been found to be expressed

in epithelial cells in the gastrointestinal tract (23). The NOX family's function is to produce H_2O_2 or superoxide (24). Among these, NOX4, *DUOX1* and *DUOX2* exclusively produce H_2O_2 (20). *DUOXA2* is the activation protein of *DUOX2*, and forms a covalent complex with *DUOX2*, which is a key factor in the formation of H_2O_2 (25). It has been reported that *DUOX2* mRNA and protein are overexpressed in CRC tissues, when compared with the normal colonic mucosa, and that the upregulation of *DUOX2* is correlated with poor prognosis (26–28). Based on existing studies, it has been speculated that *DUOX2* promotes the occurrence and development of CRC cells by producing excessive ROS and enhancing oxidative stress in the microenvironment.

RPL3 belongs to the L3P family of ribosomal proteins (RPs), and is located in the cytoplasm. As key members of the body for protein synthesis, RP family plays an important role in the process of genetic information transfer, which not only participates in the composition of translation mechanisms, but also implicates a variety of biological functions (29). For instance, RP can affect the growth, senescence, apoptosis, invasion, radiation and drug therapy resistance of cancer cells through various mechanisms. Previous studies have revealed that both hematopoietic and non-hematopoietic cancer cell lines with increased RPL3 expression exhibit enhanced sensitivity to drugs (30), while the loss of RPL3 makes chemotherapy drugs ineffective (31). RPL3 can upregulate p21 expression at the transcriptional level (31), and participate in the cell response to chemotherapy, acting as a critical regulator of the cell cycle, apoptosis and DNA repair (31). It has been found that the expression of RPL3 in CRC tissues is downregulated, when compared with the adjacent normal tissues (32). These results suggest that RPL3 is an anticancer gene. Previous studies on RPL3 have mainly focused on nucleolar stress, but the function of RPL3 in tumor invasion or metastasis remains unclear. The TCGA database revealed that there is no significant correlation between the gene expression of *DUOX2* and RPL3 in CRC (Supplementary Figure I, available at *Carcinogenesis* Online). The present study revealed that there is negative correlation between *DUOX2* and RPL3 at the protein level, while there is no significant correlation at the gene level, which is consistent with the TCGA database. It was initially demonstrated that RPL3 is one of interaction proteins of *DUOX2*, which can jointly regulate the ability of invasion and metastasis of CRC cells for the first time.

The PI3K/AKT signaling pathway promotes cell growth by inhibiting apoptosis of various cancer cells (33), and has a variety of functions, such as regulating cell growth and proliferation, promoting the progression of the cell cycle, and participating in vascular formation (34). In the present study, after the knockout of *DUOX2* with si1 and si2, the changed genes were enriched in different pathways, and PI3K/AKT was in the top four pathways. Therefore, it was considered that *DUOX2* affects the function of the PI3K/AKT pathway. Further studies have shown that RPL3 can reverse the effects of *DUOX2* on several proteins through this pathway. Hence, it could be concluded that *DUOX2* modulates the PI3K/AKT pathway through RPL3, thereby affecting the invasion ability of tumor cells.

Some previous works have reveal the potential role of *DUOX2* in the epithelia-mesenchymal transition (EMT) of CRC cells lines (15). EMT endures cells with the ability of metastasis and invasion, and it is often expressed as the upregulation of N-cadherin and downregulation of E-cadherin (35), which are regarded as landmark events of EMT (36). EMT is the key process for the invasion and metastasis of tumor cells in a variety of malignancies, such as breast cancer (37), CRC (38), prostate cancer (39) and lung cancer (40). In the present study, it was found that after the

overexpression of DUOX2, E-cadherin significantly decreased. The trend exhibited by E-cadherin was reversed after RPL3 was simultaneously increased, suggesting that DUOX2 may play an important role in the EMT process. In conclusion, DUOX2 affects the invasion and metastasis abilities of CRC cells through multiple pathways.

In summary, the present study revealed that DUOX2 has a significantly higher expression in CRC tumor samples, and facilitated the invasion and metastasis abilities of CRC cells by interacting with RPL3 and activating the AKT signaling pathway. The present study provided a new perspective on DUOX2 in regulating the occurrence and development of CRC. DUOX2 may be a prognostic factor and a potential therapeutic target for CRC in the future.

Supplementary material

Supplementary data are available at Carcinogenesis online. Supplementary Figure. (A) Statistical figures for Figure 3H and I. (B) Phase-contrast and fluorescence images of lentivirus-infected HCT116 and HT29 cells. (C) Nude mice subcutaneously injected with HCT116 cells. (D) After injection of HCT116 cells into the front flank 4 weeks later, the transplanted tumors were sacrificed and weighed. There was no difference between sh-DUOX2 and sh-Control. ^{N.S}P >0.05. (E–G) Lung and liver tissues were taken from nude mice that received lentivirus-infected HCT116 and HT29 cells for tail vein injection. (H) The expressions of DUOX2 and RPL3 protein in different tissues of CRC patients by immunohistochemistry as a supplement to Figure 3. (I) The relationship of the gene expressions of DUOX2 and RPL3 in CRC in publicly available datasets. The data were collected from the TCGA (<http://gepia.cancer-pku.cn/detail.php?gene=>). Supplementary Table 1. Gene primers used in this study Supplementary Table 2. Expression of DUOX2 in para-cancer, cancer, metastatic lymph node and metastatic liver tissue Supplementary Table 3. The candidate proteins in IP group by MS analysis

Funding

This work was supported by the Natural Science Foundation of China (grant no. 81772550 and 81502032), the Youth outstanding foundation of Hebei Province (grant no. H2019206697), the Health and Family Planning Commission of Hebei Province (grant no. 220180584) and the Key project of Hebei Province Health and Family Planning Commission (grant no. G201735).

Acknowledgements

The authors would like to thank Dr Chunyan Ding for the IHC technical help, and the Experimental Animal Center of the Fourth Hospital of Hebei Medical University for helping with the animal experiments.

Conflict of Interest Statement: The authors disclose no conflict of interest.

References

- Bray, F. et al. (2018) Global cancer statistics 2018: GLOBOCAN estimates of incidence and mortality worldwide for 36 cancers in 185 countries. *CA Cancer J. Clin.*, 68, 394–424.
- Chen, W. et al. (2016) Cancer statistics in China, 2015. *CA Cancer J. Clin.*, 66, 115–132.
- Courtney, R.J. et al. (2013) A population-based cross-sectional study of colorectal cancer screening practices of first-degree relatives of colorectal cancer patients. *BMC Cancer*, 13, 13.

- Landry, W.D. et al. (2014) ROS signalling, NADPH oxidases and cancer. *Biochem. Soc. Trans.*, 42, 934–938.
- Kizys, M.M.L. et al. (2017) DUOX2 mutations are associated with congenital hypothyroidism with ectopic thyroid gland. *J. Clin. Endocrinol. Metab.*, 102, 4060–4071.
- Jiang, H. et al. (2016) High prevalence of DUOX2 gene mutations among children with congenital hypothyroidism in central China. *Eur. J. Med. Genet.*, 59, 526–531.
- Matsuo, K. et al. (2016) High prevalence of DUOX2 mutations in Japanese patients with permanent congenital hypothyroidism or transient hypothyroidism. *J. Pediatr. Endocrinol. Metab.*, 29, 807–812.
- Wang, J. et al. (2015) PKC α promotes generation of reactive oxygen species via DUOX2 in hepatocellular carcinoma. *Biochem. Biophys. Res. Commun.*, 463, 839–845.
- Wu, Y. et al. (2011) Up-regulation and sustained activation of Stat1 are essential for interferon-gamma (IFN-gamma)-induced dual oxidase 2 (Duox2) and dual oxidase A2 (DuoxA2) expression in human pancreatic cancer cell lines. *J. Biol. Chem.*, 286, 12245–12256.
- Wu, Y. et al. (2016) Dual oxidase 2 and pancreatic adenocarcinoma: IFN- γ -mediated dual oxidase 2 overexpression results in H₂O₂-induced, ERK-associated up-regulation of HIF-1 α and VEGF-A. *Oncotarget*, 7, 68412–68433.
- Wu, Y. et al. (2013) Functional activity and tumor-specific expression of dual oxidase 2 in pancreatic cancer cells and human malignancies characterized with a novel monoclonal antibody. *Int. J. Oncol.*, 42, 1229–1238.
- Pettigrew, C.A. et al. (2012) DUOX enzyme activity promotes AKT signalling in prostate cancer cells. *Anticancer Res.*, 32, 5175–5181.
- Luxen, S. et al. (2008) Silencing of DUOX NADPH oxidases by promoter hypermethylation in lung cancer. *Cancer Res.*, 68, 1037–1045.
- Nguyen, D.M. et al. (2015) Contribution of dual oxidase 2 (DUOX2) to hyper-radiosensitivity in human gastric cancer cells. *Radiat. Res.*, 184, 151–160.
- Kang, K.A. et al. (2018) DUOX2-mediated production of reactive oxygen species induces epithelial mesenchymal transition in 5-fluorouracil resistant human colon cancer cells. *Redox Biol.*, 17, 224–235.
- Li, M. et al. (2018) Differentially expressed lncRNAs and mRNAs identified by NGS analysis in colorectal cancer patients. *Cancer Med.*, 7, 4650–4664.
- Li, J. et al. (2020) The lncRNA FEZF1-AS1 promotes the progression of colorectal cancer through regulating OTX1 and targeting miR-30a-5p. *Oncol. Res.*, 28, 51–63.
- Lin, S.C. et al. (2017) High immunoreactivity of DUOX2 is associated with poor response to preoperative chemoradiation therapy and worse prognosis in rectal cancers. *J. Cancer*, 8, 2756–2764.
- Massagué, J. et al. (2016) Metastatic colonization by circulating tumour cells. *Nature*, 529, 298–306.
- Meitzler, J.L. et al. (2019) Hydrogen peroxide-producing NADPH oxidases and the promotion of migratory phenotypes in cancer. *Arch. Biochem. Biophys.*, 675, 108076.
- MacFie, T.S. et al. (2014) DUOX2 and DUOX2A2 form the predominant enzyme system capable of producing the reactive oxygen species H₂O₂ in active ulcerative colitis and are modulated by 5-aminosalicylic acid. *Inflamm. Bowel Dis.*, 20, 514–524.
- Grasberger, H. et al. (2015) Increased expression of DUOX2 is an epithelial response to mucosal dysbiosis required for immune homeostasis in mouse intestine. *Gastroenterology*, 149, 1849–1859.
- Chu, F.F. et al. (2017) Deficiency in Duox2 activity alleviates ileitis in GPx1- and GPx2-knockout mice without affecting apoptosis incidence in the crypt epithelium. *Redox Biol.*, 11, 144–156.
- Yu, T. et al. (2018) Inhibition of NADPH oxidase activities ameliorates DSS-induced colitis. *Biochem. Pharmacol.*, 158, 126–133.
- Korzeniowska, A. et al. (2019) Functional characterization of DUOX enzymes in reconstituted cell models. *Methods Mol. Biol.*, 1982, 173–190.
- Qi, R. et al. (2016) DUOX2 expression is increased in Barrett esophagus and cancerous tissues of stomach and colon. *Gastroenterol. Res. Pract.*, 2016, 1835684.

27. Abdul, A. et al. (2016) A 19-gene expression signature as a predictor of survival in colorectal cancer. *BMC Med. Genomics*, 9, 58.
28. Wang, R. et al. (2011) NADPH oxidase overexpression in human colon cancers and rat colon tumors induced by 2-amino-1-methyl-6-phenylimidazo[4,5-b]pyridine (PhIP). *Int. J. Cancer*, 128, 2581–2590.
29. Cuccurese, M. et al. (2005) Alternative splicing and nonsense-mediated mRNA decay regulate mammalian ribosomal gene expression. *Nucleic Acids Res.*, 33, 5965–5977.
30. Hawley, R.G. (2017) Correlating chemical sensitivity with low level activation of mechanotransduction pathways in hematologic malignancies. *Explor. Res. Hypothesis Med.*, 2, 63–67.
31. Esposito, D. et al. (2014) Human rpl3 plays a crucial role in cell response to nucleolar stress induced by 5-FU and L-OHP. *Oncotarget*, 5, 11737–11751.
32. Russo, A. et al. (2016) Enhancement of 5-FU sensitivity by the proapoptotic rpl3 gene in p53 null colon cancer cells through combined polymer nanoparticles. *Oncotarget*, 7, 79670–79687.
33. Amaravadi, R.K. (2015) Transcriptional regulation of autophagy in RAS-driven cancers. *J. Clin. Invest.*, 125, 1393–1395.
34. Francesca, F. et al. (2014) A novel functional interplay between Progesterone Receptor-B and PTEN, via AKT, modulates autophagy in breast cancer cells. *J. Cell. Mol. Med.*, 18, 2252–2265.
35. Marcucci, F. et al. (2016) Epithelial-mesenchymal transition: a new target in anticancer drug discovery. *Nat. Rev. Drug Discov.*, 15, 311–325.
36. Klymkowsky, M.W. et al. (2009) Epithelial-mesenchymal transition: a cancer researcher's conceptual friend and foe. *Am. J. Pathol.*, 174, 1588–1593.
37. Joerna, F.L. et al. (2016) EMT in breast carcinoma—a review. *J. Clin. Med.*, 5, 65.
38. Cao, H. et al. (2015) Epithelial-mesenchymal transition in colorectal cancer metastasis: a system review. *Pathol. Res. Pract.*, 211, 557–569.
39. Kanayama, H. (2016) Mechanism of invasion and metastasis of prostate cancer: over view. *Nihon Rinsho*, 74, 129–134.
40. Mittal, V. (2016) Epithelial mesenchymal transition in aggressive lung cancers. *Adv. Exp. Med. Biol.*, 890, 37–56.